Journal of Power Sources 412 (2019) 321–330

Contents lists available at ScienceDirect

Journal of Power Sources

journal homepage: www.elsevier.com/locate/jpowsour

Brownian-snowball-mechanism-induced hierarchical cobalt sulfide for supercapacitors

Yucheng Zhao[a,c], Zhe Shi[c], Tianquan Lin[c,d], Liumin Suo[c], Chao Wang[c], Jing Luo[a], Zhangshun Ruan[a], Chang-An Wang[a,*], Ju Li[b,c,**]

[a] State Key Lab of New Ceramics and Fine Processing, School of Materials Science and Engineering, Tsinghua University, Beijing, 100084, PR China
[b] Department of Nuclear Science and Engineering, Massachusetts Institute of Technology, Cambridge, MA, 02139, USA
[c] Department of Materials Science and Engineering, Massachusetts Institute of Technology, Cambridge, MA, 02139, USA
[d] State Key Laboratory of High Performance Ceramics and Superfine Microstructure, Shanghai Institute of Ceramics, Chinese Academy of Sciences, Shanghai, 200050, PR China

HIGHLIGHTS

- Precise control of synthesizing process for cobalt sulfide hierarchical porous nanospheres.
- Brownian snowball mechanism is put forward and supported by first-principles calculations.
- The capacitance reflects hybrid electrical energy storage.
- Largely improved EC performance could be attributed to the unique architecture.

GRAPHICAL ABSTRACT

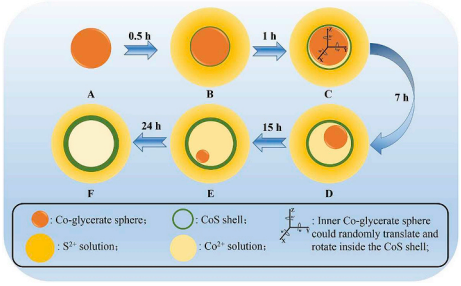

ARTICLE INFO

Keywords:
Supercapacitor
Cobalt sulfide
Hierarchical porous nanospheres
Brownian snowball mechanism
Precise control
Differentiate Faradaic capacitance

ABSTRACT

Transition metal sulfides with hierarchical (ball in ball) micro/nanoporous structures have drawn wide spread interests for various applications, such as energy storage, catalysis, solar cells, owing to their unique features and intriguing properties. However, precise control of synthesizing process for hierarchical porous nanospheres of transition metal sulfides remains a big challenge. In addition, the charging and discharging process of transition metal sulfides in electrochemical storage is still a black box. Herein we design and precise control of synthesizing a transition metal sulfide with hierarchical porous nanosphere structure, namely cobalt sulfide hierarchical porous nanospheres (HPNs). Brownian snowball mechanism is put forward to explain the formation mechanism of CoS samples, which is supported by first-principles calculations. The proposed Brownian snowball mechanism helps us understand the formation process and facilitates comprehensive and precise manipulation, a key requirement for industrial scale-up. The CoS hierarchical porous nanospheres with a specific surface area of approximately 140 m^2/g possess a total specific capacitance of 1310 F/g and 932 F/g at a current density of 5 A/g when used as electrode materials for electrochemical capacitors. The capacitance reflected hybrid electrical energy storage and is separated into double layer charging and the Faradaic contribution from the OH^- ions reactions with surface atoms. It is demonstrated that Faradaic capacitance dominates in CoS hierarchical porous nanospheres exceeding 770 F/g by an analysis of the voltammetric sweep data.

* Corresponding author.
** Corresponding author. Department of Materials Science and Engineering, Massachusetts Institute of Technology, Cambridge, MA 02139, USA.
E-mail addresses: wangca@mail.tsinghua.edu.cn (C.-A. Wang), liju@mit.edu (J. Li).

https://doi.org/10.1016/j.jpowsour.2018.11.055
Received 4 June 2018; Received in revised form 12 November 2018; Accepted 16 November 2018
0378-7753/

1. Introduction

Transition metal sulfides (TMS) are investigated for catalysis [1], solar cells [2] and energy storage [3]. Supercapacitors and batteries are the two categories of electrical energy storage [4–9]. Recently, TMS have attracted soaring popularity for supercapacitors because of their high energy density, good cycling performance, and excellent conductivity [10–17]. Among TMS, various cobalt sulfide compositions with porous and hierarchical structures have been investigated owing to their superior pseudocapacitive properties [17–33]. Co_3S_4 hollow nanostructures grown on graphene presents a specific capacitance of 521.7 F/g at 5 A/g [10]. CoS hollow nanocube structures manifest good Faradaic performance [13]. Ultra-long $CoS_{1.097}$ nanotubes networks have been synthesized for supercapacitors [21]. When working within the thermodynamic voltage stability window of the liquid electrolyte, no solid-electrolyte interface (SEI) will form on the electrode, in which case a high surface-to-volume ratio should be beneficial for high rate performance. Based on this philosophy, we would like to study mesoporous hollow architectures of cobalt sulfides. Meanwhile, cobalt sulphides show 0 eV band gap which make them excellent candidate for electrode materials. Although various cobalt sulfide nanostructures have been synthesized for supercapacitors, barely any work elaborated on the detailed formation mechanism of these nanostructures. Studying the formation mechanism of spherical architectures would facilitate precise control of fabrication and differentiate Faradaic capacitance of electrode material may instruct further design and manufacture for enhanced supercapacitors.

Herein, we report an anion-cation exchange method to precisely fabricate innovative cobalt sulfide hierarchical porous nanospheres with high specific surface area, consisting of solvothermal synthesis of cobalt glycerate followed by sulfidation in the presence of thioacetamide to acquire CoS hierarchical porous nanospheres (CoS-HPNs). By adjusting the sulfidation time, temperature and concentration of mixed reagents which are involved in the solvothermal reaction, the inner structure of the CoS-HPNs could be easily adjusted and controlled accurately. We subsequently proposed a “Brownian snowball mechanism” to explain the high sphericity of CoS-HPNs. First-principles calculations reveal that outward Co diffusion is faster than inward S diffusion, implying that the CoS yolk-shell (YS) structure forms on the outer surface of former shell which proves the Brownian snowball mechanism. Investigating electrochemical charge storage mechanism, the Faradaic capacitance effects accounts 59.3% of the total capacitances (1310 F/g), indicating that improving specific surface area of CoS-HPNs is also necessary.

2. Experimental

2.1. Synthesis of the CoS hierarchical porous nanospheres

Analytically pure commercial chemical reagents were used. In a representative synthesis, 0.5 mmol of $CoCl_2{\cdot}6H_2O$ (Alfa Aesar), 10 ml of glycerol (Sigma Aldrich) were dispersed into 70 ml isopropanol (Alfa Aesar) and the solution was ultrasonicated for 10 min until a transparent pink solution was finally formed. The solution was then transferred into a 100 ml capacity Teflon stainless steel autoclave and maintained at 120 °C for 5 h. After cooling down naturally to room temperature (around 23 °C), the brown-pink precipitates were treated with centrifugation at 10000 r/min for 2 min, washed with deionized water and ethanol alternately for 3 times and dried in an oven at 60 °C for 4 h. And the Co-glycerate powders were prepared successfully. For the preparation of CoS-HPNs, 30 mg Co-glycerate and thioacetamide (Sigma Aldrich) were added into 20 ml ethanol (Sigma Aldrich) and the solution must be ultrasonicated for 10 min until all the thioacetamide was dissolved. The mixture was transferred into a 100 ml capacity Teflon stainless steel autoclave and kept at a different temperature, amount of thioacetamide and sulfidation periods. After cooling down naturally to room temperature (around 23 °C), the black precipitates were treated with centrifugation at 10000 r/min for 3 min, washed with deionized water and ethanol alternately for both 3 times and dried in an oven at 60 °C for 4 h, the CoS-HPNs were obtained.

2.2. Synthesis of the Mn—Co—S hierarchical porous nanospheres

In a representative synthesis, 0.5 mmol of $CoCl_2{\cdot}6H_2O$ (Alfa Aesar), 0.25 mmol of $MnCl_2{\cdot}4H_2O$ (Alfa Aesar) and 10 ml of glycerate (Sigma Aldrich) were dispersed into 70 ml isopropanol (Alfa Aesar), and the solution shall be ultrasonicated for 10 min until a transparent pink solution is finally formed. The solution was then transferred into a 100 ml capacity Teflon stainless steel autoclave and maintained at 120 °C for 5 h. After cooling down naturally to room temperature (around 23 °C), the precipitates were treated with centrifugation at 10000 r/min for 2 min, washed with deionized water and ethanol alternately for 3 times and dried in an oven at 60 °C for 4 h. For the preparation of Mn—Co—S hierarchical porous nanospheres, 30 mg MnCo-glycerate and thioacetamide (Sigma Aldrich) were added into 20 ml ethanol (Sigma Aldrich) and the solution must be ultrasonicated for 10 min until all the thioacetamide was dissolved. The mixture was transferred into a 100 ml capacity Teflon stainless steel autoclave and kept at different temperature, amount of thioacetamide and sulfidation periods. After cooling down naturally to room temperature (around 23 °C), the black precipitates were treated with centrifugation at 10000 r/min for 3 min, washed with deionized water and ethanol alternately for three times and dried in an oven at 60 °C for 4 h, the Mn—Co—S hierarchical porous nanospheres were obtained.

2.3. First-principles calculations

The calculations were performed using the Vienna Ab initio Simulation Package [34] code based on density functional theory (DFT). We used the Perdew-Burke-Ernzerhof [35] exchange-correlational functional and the projector augmented wave method [36] in our calculations. A plane wave basis set with an energy cutoff of 300 eV was used to expand the electronic wavefunctions. The Brillouin zone integration was conducted on a 4×4×4 Monkhorst-Pack [37] k-point mesh. Atomic coordinates in all structures were relaxed until the maximum residual force was below 0.02 eV $Å^{-1}$. The optimized lattice constant is 9.18 Å for the unit cell of Co_3S_4, which is in agreement with other computational [43] and crystallographic data (Co_3S_4 Crystal Structure: Datasheet from “PAULING FILE Multinaries Edition-2012” in Springer Materials (http://materials.springer.com/isp/crystallographic/docs/sd_0556901), Springer-Verlag Berlin Heidelberg & Material Phases Data System (MPDS), Switzerland & National Institute for Materials Science (NIMS), Japan.). Either Co or S vacancy was created and allowed to migrate in the material to simulation diffusion in solid phase Co_3S_4, during which energy barrier was computed by the Nudged Elastic Band (NEB) [38] method.

2.4. Materials characterization

Microstructure of the nanospheres was examined by using a transmission electron microscope (TEM) (Tecnai G220) in the bright field at 200 kV for images and field emission scanning transmission electron microscopy (FESEM) (JEOL, JSM-7800F). TEM was also used for EDS mapping. The X-ray diffraction (XRD) data were acquired by a Bruker XRD (D8 ADVANCE A25) with Cu Kα ($\lambda = 0.154178$ nm) radiation. The diffraction patterns were recorded from 10° to 90° at a scanning rate of 5°/min. X-ray photoelectron spectroscopy (XPS) data were obtained through an ESCALAB 250 Xi electron spectrometer from VG Scientific using 300 W Al Ka radiation. The base pressure was approximately 3×10^{-9} mbar. The Brunauer-Emmett-Teller surface area and pore structure analysis were measured on an Autosorb-iQ2-MP surface area and porosimetry analyzer.

2.5. Electrochemical measurements

The cathode slurry was prepared by mixing ethanol with CoS-HPNs powder only (no binder or conductive agents). Then the slurry was pressed onto nickel foam (round sheet with radius $r = 7$ mm) at a pressure of 25 t, and then dried at 70 °C for 3 h. The typical mass loading of CoS-HPNs electrode materials in each nickel foam sheet is about 2.5 mg/cm^2. The tap density of the CoS-HPNs is 0.35 g/cm^3. With a pressure of 25 t, the compacted density of the CoS-HPNs is 2.073 g/cm^3 if pressed against a hard nonporous substrate.

Electrochemical measurements were conducted on a CHI 760E electrochemical workstation in 3 M NaOH aqueous electrolyte in a three-electrode system, where a platinum foil serving as the counter electrode (−) and a saturated calomel electrode (SCE) as the reference electrode. We will use symbol $U_{\pm}$ to denote the measured *electrode* voltage of cathode and anode with respect to a reference electrode (SCE here), and use symbol

$$V \equiv U_+ - U_- \tag{S1}$$

to denote the measured *cell* voltage. We will use $Q \equiv Q_+ = Q$- (unit Coulomb) to denote the charge transfer from anode to cathode. The cathode's differential capacitance will be denoted by lower-case

$$c_+ \equiv \frac{1}{m_+}\frac{dQ}{dU_+} \tag{S2}$$

where m_+ is the mass of the cathode-active material (in g) without the Ni-foam current collector. In this work we always use CoS-HPNs as the cathode. Differential capacitance can also be defined for the anode,

$$c_- \equiv -\frac{1}{m_-}\frac{dQ}{dU_-} \tag{S3}$$

although in "half-cell tests" we do not care very much about what happens on the anode side as long as its reaction kinetics is facile enough in providing the sources and sinks for the OH^- and e^- that one needs for the cathode reactions. c_+ is generally not a constant and depends on U_+, so we can define an average capacitance

$$\overline{c_+} \equiv \frac{1}{m_+}\frac{\Delta Q}{\Delta U_+} = \frac{1}{m_+}\frac{\Delta Q}{U_+^{\text{uppercut}} - U_+^{\text{lowercut}}} = \frac{\int_{U_+^{\text{lowercut}}}^{U_+^{\text{uppercut}}} c_+(U_+)dU_+}{U_+^{\text{uppercut}} - U_+^{\text{lowercut}}} \tag{S4}$$

over the voltage range $[U_+^{\text{lowercut}}, U_+^{\text{uppercut}}]$ that the cathode experiences. When we perform galvanostatic charge/discharge with constant current I, we get

$$c_+ = \frac{I\Delta t}{m_+(U_+^{\text{uppercut}} - U_+^{\text{lowercut}})} \tag{S5}$$

where Δt is the charge/discharge duration.

3. Results and discussion

3.1. Formation and calculations

With solvothermal reaction of $CoCl_2{\cdot}6H_2O$ and glycerol under 120 °C for 5 h, Co-glycerate solid spheres could be synthesized successfully, this method is modified from early report [22]. $CoCl_2{\cdot}6H_2O$ and glycerol are firstly dissolved into isopropanol totally and at a temperature of 120 °C, glycerate ($C_3H_5O_4^-$) resulted from the decomposition of glycerol ($C_3H_8O_3$) will attract Co^{2+} ions to form Co-glycerate ($Co(C_3H_5O_4)_2$) nucleus. Owing to homogenous nucleation mechanism, round and uniform Co-glycerate nanospheres (Fig. 1, stage A) could be synthesized [22] with diameter on the order of 500 nm. An anion-cation exchange method under the solvothermal condition is used to transform Co-glycerate solid precursors into CoS-HPNs. The overall transformation procedure can be illustrated schematically in Fig. 1. At stage B, Co^{2+} ions which are rich in Co-glycerate solid sphere react with S^{2-} ions decomposed from thioacetamide at 85 °C for 0.5 h on the very surface of original Co-glycerate sphere. The sulfidation process could be regarded as an anion-cation exchange reaction between Co-glycerate and thioacetamide. At stage C, after sulfidation for 1 h inward diffused S^{2-} ions and outward diffused Co^{2+} ions provide an unfailing supply of sources for the growth of cobalt sulfide shell leading to a clearly defined gap space between the shell and inner Co-glycerate. At stage E, with the progress of sulfidation for 15 h, the volume of inner Co-glycerate solid sphere become further smaller while the shell of cobalt sulfide grows thicker. After sulfidation for 24 h, the Co-glycerate sphere disappears eventually, and one whole cobalt sulfide thick shell is finally obtained at the end of stage F. The formation formula (equation (1)) is as follows:

$$Co(C_3H_5O_4)_2 + CH_3C(S)NH_2 + H_2O \xrightarrow[85°C,\ solvothermal]{CH_3CH_2OH} CoS + CH_3C(O)NH_2 + 2C_3H_6O_4 \tag{1}$$

As for stage B, C, D and E, the thin-shell particle, which is spherically symmetric at the beginning, will tumble in the liquid solution due to thermal Brownian motion and minute flow agitations, causing random gyrations and translations of the inner core which is still

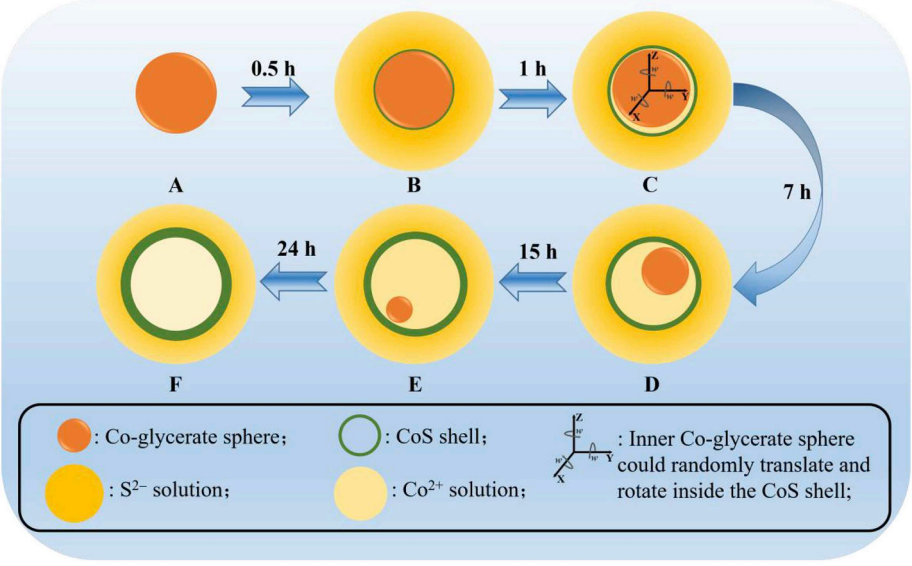

Fig. 1. Schematic illustration of the synthesis process of CoS hierarchical porous nanospheres.

immersed in an inner fluid (as the thin-shell is unlikely to be fully hermetic at the beginning). This causes dispensation of Co^{2+} and other species in a spherically symmetrical manner in the inner fluid, the further reaction of which with the outside S^{2+} will keep the spherical symmetry the shell despite thickening, like a rolling snowball. In cases where the inner core is stuck firmly on the shell and cannot randomly tumble, we have seen deformed core-shell structure as well with imperfect sphericity (Fig. 3(k1) TEM picture), but this is rare in our experiments. We call this mechanism of forming a spherical shell despite transient off-centeredness (see Fig. 3(b2-i2) TEM pictures) the "Brownian snowball mechanism". Meanwhile, the concentration of S^{2-} ions in the gap space decreases dramatically when cobalt sulfide continuously forms, and it turns hard for S^{2-} ions to diffuse into the gap space because of the barrier-like shell.

First-principles calculations were carried out to quantitatively investigate the vacancy diffusion barrier for S^{2-} and Co^{2+}. Fig. 2(a) demonstrates the proposed mechanism of forming the cobalt sulfide shell. First-principles calculations were carried out to quantitatively explain this mechanism. Typically, a diffusion process takes place in two possible manners, namely vacancy diffusion or interstitial diffusion. In a solid-state material medium, however, diffusion is primarily realized by vacancies. Thus, we can compare the energy barrier for vacancy migration through the S and Co lattice site to decide which diffusion direction is dominant in forming the shell. As shown in Fig. 2(b), it was found that migration energy required for S vacancy is higher than that of Co along the diffusion path, indicating that S^{2-} ions are much harder to get through the solid-state shell than Co^{2+}. As a result, Co vacancies in the shell would profusely move inward to allow Co^{2+} ions to move outward (Fig. 2(a) and (c)). The Co^{2+} ions inside the shell would act as a Co reservoir. Whenever a Co vacancy reached the inner shell surface a Co^{2+} in the reservoir would come to it and supply a Co^{2+} ion to sustain the diffusion process. This way, a fresh outer shell surface in excess of Co can be consistently formed from within and the reaction of Co and S would take place externally, completing the snowball-accumulating process. This echoes the experimental phenomenon that new cobalt sulfide is formed outside the shell instead of packing up at the interior, as illustrated in Fig. 2(a). Moreover, if we assume interstitial diffusion does exist, then S^{2-} and Co^{2+} ions would act by themselves as the diffusion species instead of their respective vacancies. In this manner, the same conclusion can also be drawn from energy barrier analysis, which is detailed in Fig. S1.

3.2. Morphology characterization

To further demonstrate the formation mechanism of the metal sulfide nanospheres, FESEM, TEM and powder XRD are adopted to capture the morphological evolution as a function of the sulfidation time. Fig. 3(a1, a2) shows that the Co-glycerate precursor is composed of uniform and monodispersed solid spheres with slightly wrinkled surface and no visible pores. After sulfidation reaction at 85 °C for 1 h, the color of the as-prepared CoS-1h transformed from original brown-pink into grey-black. If the sulfidation time is 3 h or more, the color turns totally black, indicating the formation of metal sulfide. As presented in Fig. 3(b1, b2), a clear gap space appears between inner Co-glycerate core and outer cobalt sulfide shell. Compared with Co-glycerate, the surface of CoS-1h has become rougher which suggests the occurrence of sulfidation reaction on the Co-glycerate surface. With the sulfidation time gains, the inner Co-glycerate sphere shrinks gradually while the diameter of outer cobalt sulfide shell increases progressively and all the Co-glycerate sphere disappears when sulfidation time reaches 24 h (Fig. 3(c1, c2) to Fig. 3(i1, i2)). EDX-elemental mapping (Fig. 3(j1, j2, j3) and Fig. 3(k1, k2, k3)) offers clear evidence about the elemental

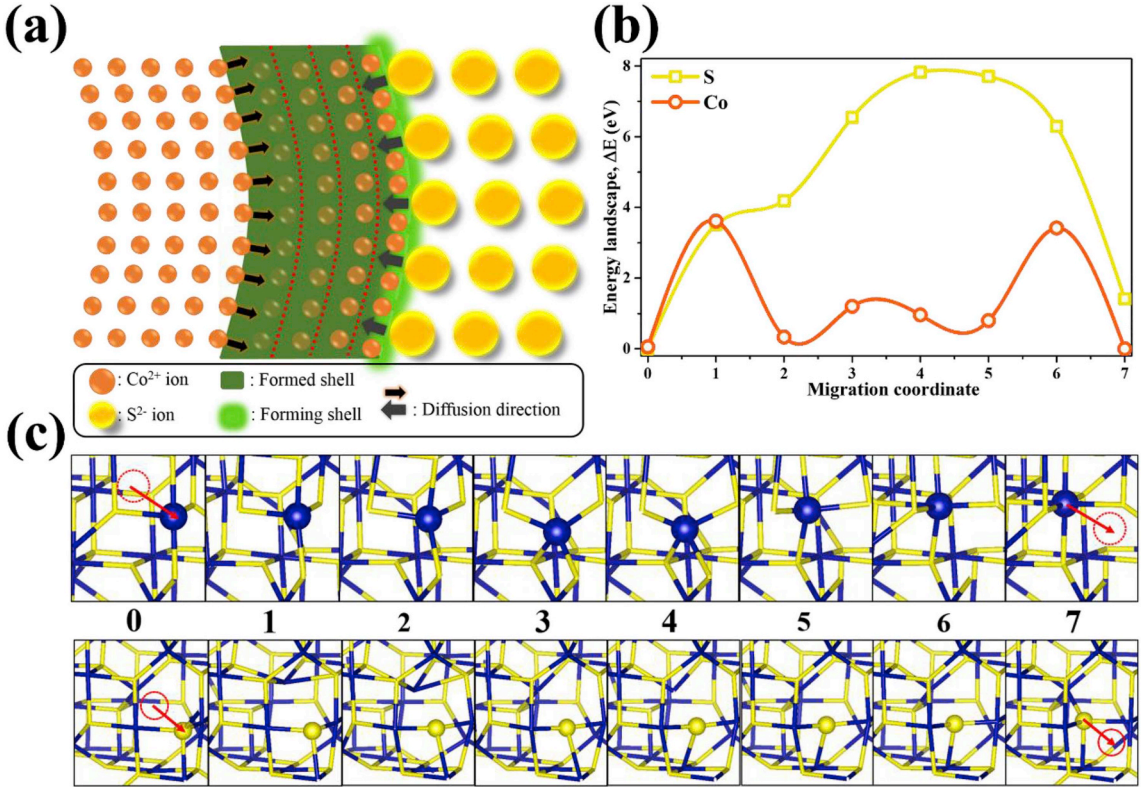

Fig. 2. DFT calculations of vacancy diffusion barrier and pathway using NEB. (a) Schematic illustration for the diffusion of Co^{2+} and S^{2-}. Co^{2+} is more favorable than S^{2-} to penetrate cobalt sulphide shell. (b) Energy change from initial to final configurations, and (c) the associated atomistic structure along the pathway for Co and S vacancy diffusion. The red circle illustrates the initial and final position of the vacancy site. One Co atom (colored in blue) and one S atom (in yellow) are drawn to show how they are displaced by the migration of vacancy. (For interpretation of the references to color in this figure legend, the reader is referred to the Web version of this article.)

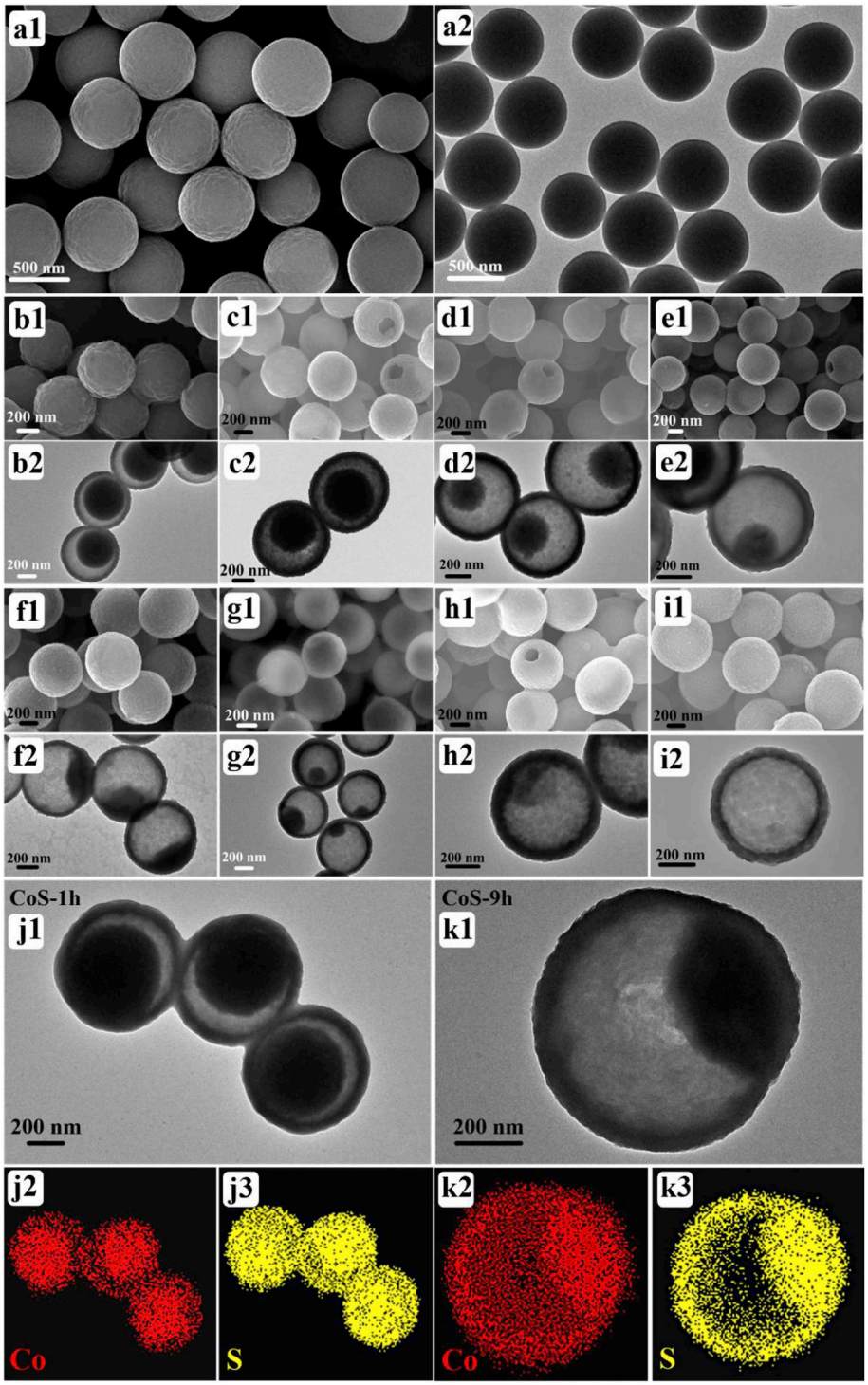

Fig. 3. FESEM, TEM and EDX-elemental mapping images of Co-glycerate and various CoS-HPNs. (a1, a2) FESEM and TEM photos of Co-glycerate solid spheres; (b1, b2) FESEM and TEM photos of CoS-1h HPNs; (c1, c2) FESEM and TEM photos of CoS-3h HPNs; (d1, d2) FESEM and TEM photos of CoS-5h HPNs; (e1, e2) FESEM and TEM photos of CoS-7h HPNs; (f1, f2) FESEM and TEM photos of CoS-9h HPNs; (g1, g2) FESEM and TEM photos of CoS-12h HPNs; (h1, h2) FESEM and TEM photos of CoS-15h HPNs; (i1, i2) FESEM and TEM photos of CoS-24h HPNs; (j1, j2, j3) TEM, cobalt and sulfur EDX-elemental mapping images of CoS-1h HPNs; (k1, k2, k3) TEM, cobalt and sulfur EDX-elemental mapping images of CoS-9h HPNs.

distribution on and within spheres. The overall distribution of cobalt and sulfur elements in the CoS-1h and CoS-9h HPNs are uniform, which verifies the formation of cobalt sulfide composites. The crystallinity of all the samples are examined by XRD which is shown in Fig. S3(a). No obvious diffraction peak could be found in the nine samples, revealing poor crystallinity of all the cobalt sulfide samples and this amorphous architecture may facilitate their electrochemical performance [31–33]. The Co-glycerate spheres are highly uniform and monodisperse with a diameter of around 500 nm, and the slightly wrinkled surface of Co-glycerate spheres could also be observed (Fig. S2). The relatively low sulfidation temperature (85 °C) for all samples induces the poor crystallinity and amorphous architecture [22]. In Fig. 3(c1, d1, e1, h1), several cobalt sulfide nanospheres are partially broken owing to thin shells. Nevertheless, (Fig. S4) the majority of CoS-HPNs remain complete and intact. The fabrication of this yolk-shell and hollow architectures could be explicitly explained by the continuous ion exchange process mostly on the outer surface of the pre-formed cobalt sulfide shell as discussed earlier. The presented “Brownian snowball” mechanism of forming hierarchical porous nanospheres is facile and quite universal. For instance, uniform and monodispersed Mn—Co-glycerate solid spheres with a diameter of about 900 nm could be fabricated by a similar solvothermal method (Fig. S5(a1, a2, a3)). The Mn—Co-glycerate solid spheres chemically transformed into Mn—Co—S hierarchical porous nanospheres after sulfidation reaction (Fig. S5(b1, b2, b3)).

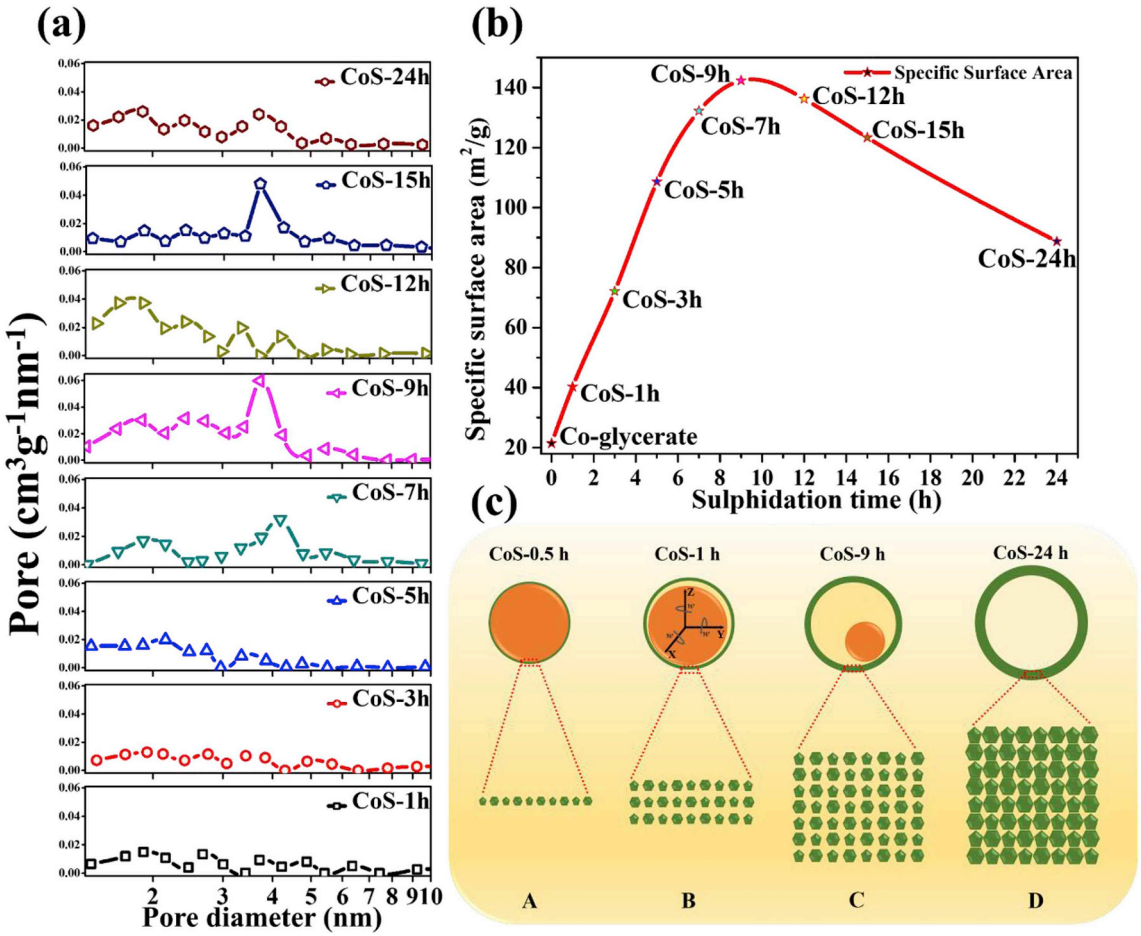

Fig. 4. (a) Pore size distribution of all CoS-HPNs; (b) Specific surface area of Co-glycerate and all cobalt sulfide samples; (c) Schematic illustration for grain growth in CoS-HPNs shell.

3.3. Precise control of the shell of CoS-HPNs

The sulfidation time, temperature and concentration of mixed reagents are taken into consideration for precise control of CoS-HPNs. Temperature and concentration of thioacetamide are two other fundamental factors in the formation process of CoS-HPNs. The hierarchical porous nanospheres acquired from sulfidation at 100 °C for 3 h are decorated with numerous small cobalt sulfide spheres (around 30 nm in diameter) scattered on the surface of original cobalt sulfide hierarchical porous nanospheres (Fig. S6) which implies higher sulfidation temperature damages uniformity of the cobalt sulfide shell. In Fig. S7(b), cobalt sulfide sphere obtained when 200 mg thioacetamide is used as a sulfur source has thicker cobalt sulfide shell and darker Co-glycerate inner spheres than normal cobalt sulfide spheres from Fig. S7(a). More long-lasting supply of sulfide ions from the decomposition of thioacetamide would accelerate the formation of outer cobalt sulfide shell and decelerate the disintegration of the inner Co-glycerate sphere which would induce a thicker and denser shell of the resulting cobalt sulfide spheres, which may lead to lower specific surface area and inferior electrochemical performance. To reveal the regularity of the changing parameters of various CoS-HPNs, specific statistics have been collected in Table S1. Two curves are presented in Fig. S9(d): one represents the diameter of Co-glycerate against the diameter of the formed cobalt sulfide shell as a function of sulfidation time and the other one manifests thickness of the shell against the formed cobalt sulfide shell as a function of sulfidation time. Two curves simultaneously signify that the Co-glycerate turns smaller while the cobalt sulfide shell gains thicker with the increasing sulfidation time. Meanwhile, the Co-glycerate inner cores in Figs. S8(e, f, g) are in the shape of ooze (brown dotted line) which implies the decreasing mechanical strength properties of the inner nanospheres owing to a continuously outward diffusion of Co^{2+} ions during sulfidation process.

3.4. Characterization of CoS-HPNs

N_2 adsorption-desorption measurements are employed to calculate the specific surface area (SSA) of Co-glycerate and all cobalt sulfide samples (Fig. S3(b) and Fig. 4(a)). Fig. 4(a) implies that pores in CoS-HPNs are mainly mesoporous and microporous, which are formed between interconnected amorphous areas and will facilitate electrochemical performance of supercapacitor. As shown in Fig. 4(b), Co-glycerate only possesses an SSA of 20 m^2/g. With the increasing sulfidation time, SSA of various CoS-HPNs increases dramatically before CoS-9h to the highest 140 m^2/g and decreases gradually to 80 m^2/g of CoS-24. Sulfidation process triggers the formation of numerous tiny cobalt sulfide grains on the surface of Co-glycerate which is in favor of improving SSA of CoS-HPNs (Fig. 4(c), A). After sulfidation for 1 h (Fig. 4(c), B), grains grow slightly bigger, porous and hierarchical shell of CoS-1h turns marginally thicker and higher SSA could be acquired compared with CoS-0.5h. However, when sulfidation reaches a critical point (~9 h) (Fig. 4(c), C), CoS grains grow larger continuously, shell of cobalt sulfide becomes thicker, the gaps between cobalt sulfide particles turns narrower, and the whole shell architecture becomes denser again because of Brownian snowball mechanism, leading to a decreased SSA afterward (Fig. 4(c) and D). Furthermore, the oxidation states of cobalt and sulfur are investigated by XPS. Full-survey-scan spectrum (Fig.

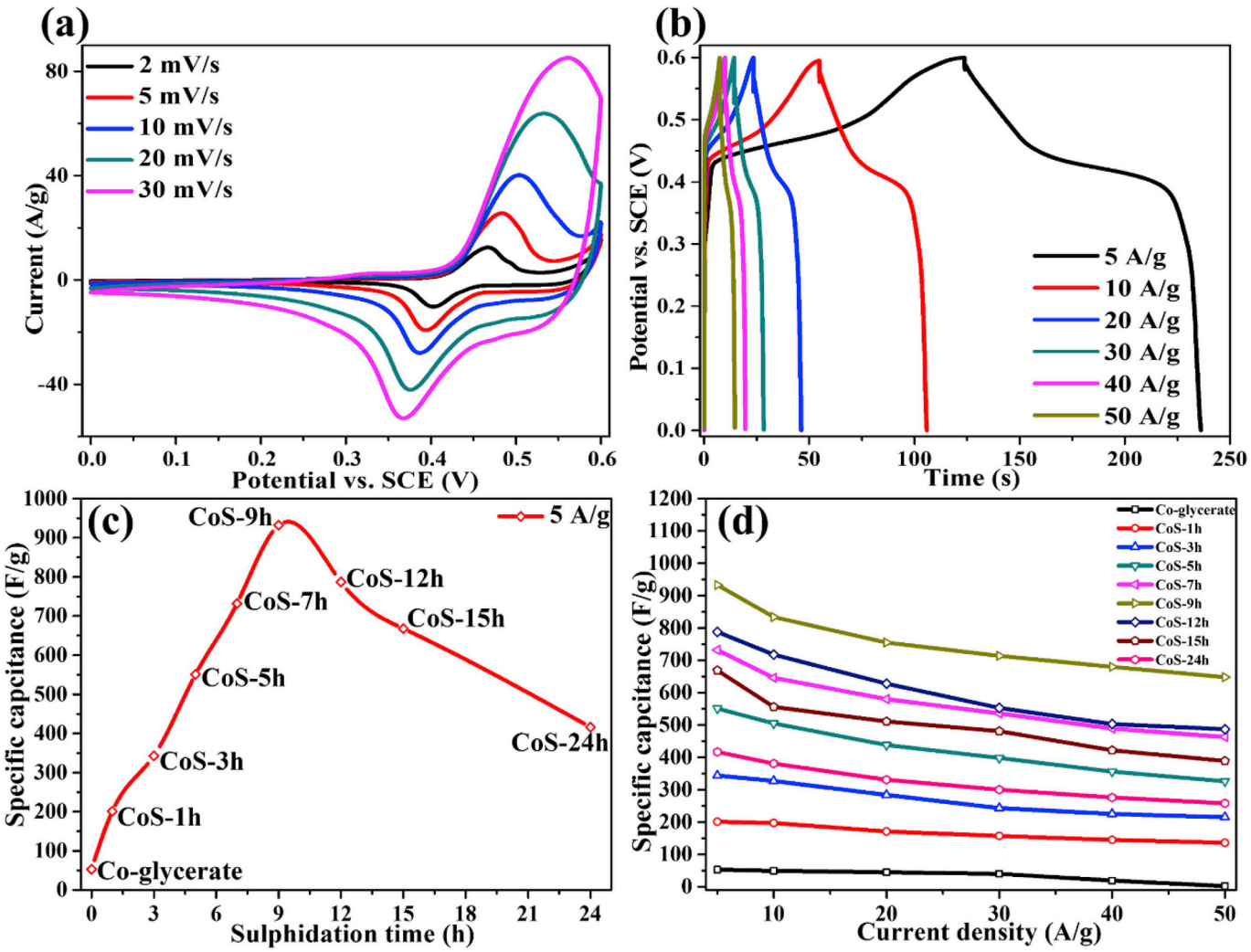

Fig. 5. Electrochemical properties of CoS-hierarchical porous nanospheres. (a) CV curves of CoS-9h; (b) Galvanostatic charge/discharge (GCD) curves of CoS-9h; (c) Comparison of specific capacitances of cobalt sulfide spheres at 5 A/g; (d) Rate capability of cobalt sulfide spheres at various current densities.

S9(a)) confirms the presence of Co and S elements in CoS-3h, CoS-9h and CoS-15h and absence of S element in Co-glycerate. Figs. S9(b and c) displays high-resolution XPS spectra of Co and S elements. For CoS-9h, the peak centered at around 779.16 eV and 794.26 eV are evident of cobalt sulfide of Co $2p_{3/2}$ and Co $2p_{1/2}$ in the composites. The gap between Co $2p_{3/2}$ and Co $2p_{1/2}$ peaks is 15.10 eV which matches the standard spin-orbit coupling of Co $2p_{3/2}$ and Co $2p_{1/2}$. The S 2p peak at 162.73 eV corresponds to the spin-orbit coupling in cobalt sulfide [25].

3.5. Electrochemical measurements of CoS-HPNs

We use 3 mol/L NaOH aqueous electrolyte. The typical Cyclic Voltammogram (CV) curves of the CoS-9h-HPNs electrode at various scan rates ranging from 2 to 30 mV/s in a voltage window of 0–0.6 V versus SCE are provided in Fig. 5(a). The CV curves demonstrate a set of symmetric Faradaic charging/discharging peaks, signifying the presence of redox reactions of cobalt sulfide during the charge and discharge process. Even with a 15-fold increment in scan rate, from 2 to 30 mV/s, there is no large change in the shape and position of redox peaks, indicating that the redox reactions have fast charging/discharging kinetics. These obvious redox peaks might be attributed to the reversible Faradaic redox processes of $Co^{2+}/Co^{3+}/Co^{4+}$ based on the following reactions (equations (2.1) and (2.2)) [21,22]:

$$CoS + OH^- \underset{\text{Discharging}}{\overset{\text{Charging}}{\rightleftarrows}} CoSOH + e^- \quad (2.1)$$

$$CoSOH + OH^- \underset{\text{Discharging}}{\overset{\text{Charging}}{\rightleftarrows}} CoSO + H_2O + e^- \quad (2.2)$$

Consistent with the CV results, all galvanostatic charge/discharge tests (Fig. 5(b)) show symmetric features with a step derived from the Faradaic redox. A specific capacitance as high as 932 F/g at a current density of 5 A/g was obtained for CoS-9h. Over a wide range of current densities, CoS-9h continued to provide a well-behaving galvanostatic charge/discharge curve and high capacitance, achieving 650 F/g at 50 A/g, which is much higher than known EDLC and quite comparable to the capacitance of transition metal-oxide faradaic pseudocapacitors. Comparing with other samples prepared by different sulphidation time, shown in Fig. 5(c), the sample obtained by 9 h marked as CoS-9h possesses the best performance due to its highest specific surface area and electronic conductivity. Rate capabilities of all samples are graphed in Fig. 5(d) with a current density of 5 A/g to 50 A/g. CoS-9h owns the highest specific capacitances at all current densities and with the increase of current density, the specific capacitance of CoS-9h electrode decreases gradually, but still keeping a high value of 650 F/g even at 50 A/g. Approximately 70% of capacitance for CoS-9h is retained when the current density is elevated from 5 to 50 A/g. Compared with CoS-9h,

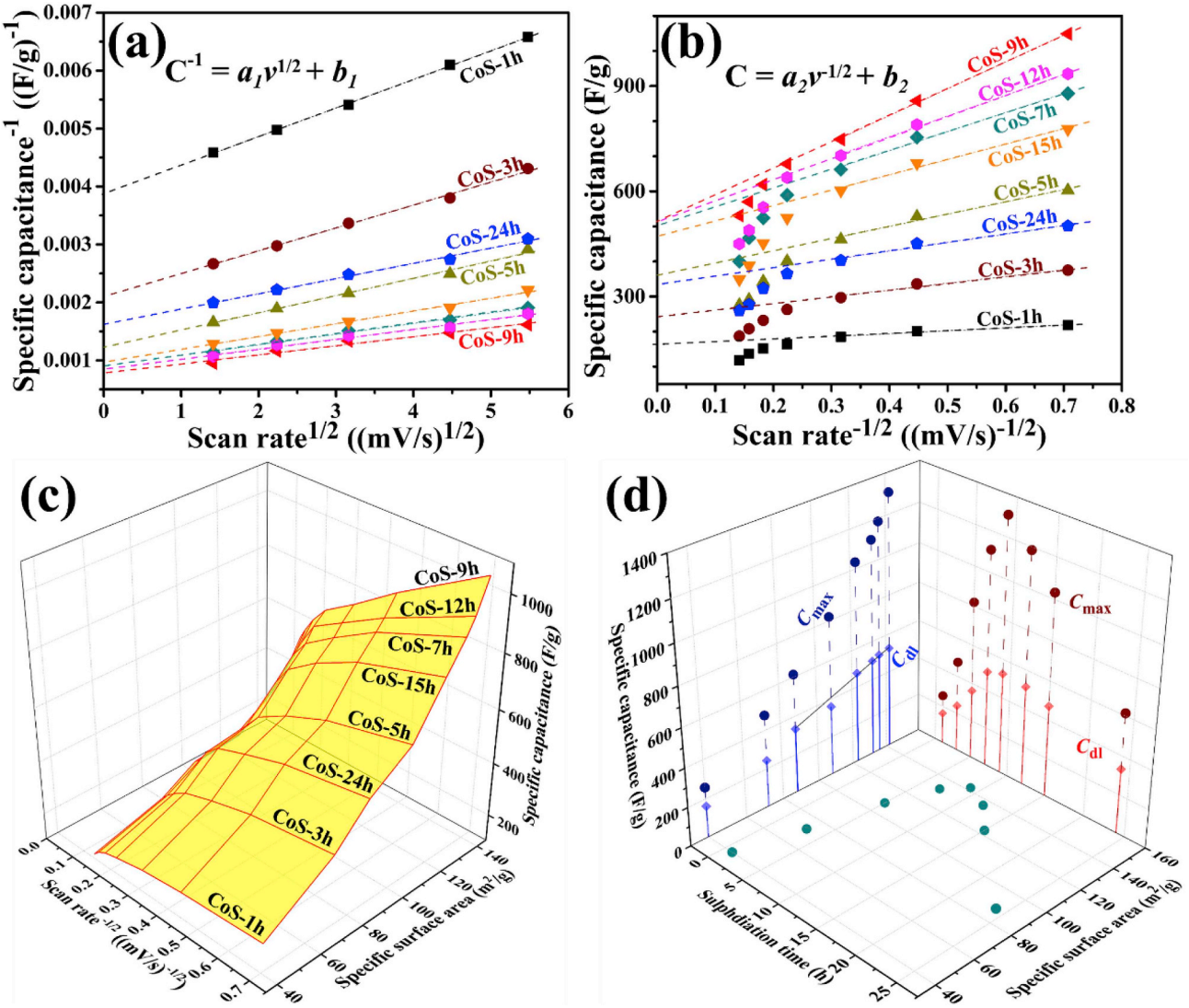

Fig. 6. Electrochemical mechanism analysis of CoS-hierarchical porous nanospheres. (a) Reciprocal of specific capacitance versus square root of scanning rates, $v^{1/2}$, the extrapolation of capacitance to $v = 0$ is given the total capacitance. (b) Specific capacitance *vs.* root-inverse sweep rate, $v^{-1/2}$, with v from 2 to 50 mV/s; Extrapolated intercept capacitance is rate-independent capacitance, the remainder diffusion-controlled capacitance. (c) 3D surface plot of specific capacitance, root-inverse sweep rate ($v^{-1/2}$), and specific surface area. (d) 3D scatter plot of specific capacitance, specific surface area, and sulphidation time.

other samples display inferior electrochemical performance. However, their rate capabilities are still good relative to other materials. The robust redox reactions established in all samples confirmed by the cycling test at a high current density of 10 A/g for 1000 cycles (Fig. S10a). After that, the retention of all electrode materials remains well above 90%, some of them even reach over 100%. The excellent cycling ability stem from their unique hierarchical porous and amorphous architectures. Electrochemical impedance spectroscopy (Fig. S10(b)) found Co-9h to have very low equivalent series resistance of ~0.4 ohms. This may be attributed to better contacting to electrolyte, because of the unique hierarchical porous architectures. High conductivity is a guarantee for obtaining excellent rate capability which is critical in supercapacitors requiring high power density and energy density simultaneously.

The total capacitance can be separated into two components: the Faradaic contribution from the OH^- ions reaction process, referred to as pseudocapacitance, the nonFaradaic contribution from the electric double layer (EDL) effect. In the partition procedure, the total voltammetric specific capacitance, C_T, is given from the extrapolation of voltammetric charge, C, to scan rate $v = 0$ from the plot of 1/C vs. $v^{1/2}$ (see Fig. 6(a)). Here, we can obtain the total voltammetric specific capacitance C_T = 1310 F/g for CoS-9h hierarchical porous nanospheres and C_T = 1185 F/g for CoS-7h, C_T = 1110 F/g for CoS-12h.

To investigate the electrochemical charge storage mechanisms, we next use the method of Conway [39] and Dunn [40,41] to quantitatively separate the contribution. Fig. 6(b and c) reveals the analysis to establish the charge-storage mechanism for CoS hierarchical porous nanospheres electrode. Assuming that the current (i) obeys a power-law relationship with the sweep rate (v) leads to two parts (equation (3)) [42]:

$$i = av^b \tag{3}$$

Both a and b are adjustable parameters, with b-values determined from the slope of the plot of log i vs. log v. There are two well-defined conditions: $b = 0.5$ is indicative of a Faradaic process while $b = 1.0$ is representative of a capacitive response. At the peak potential, the b-value is 0.65, indicating that the current comes primarily from the OH^- ion reaction.

A closer examination of the voltammetric sweep rate dependence enables one to distinguish quantitatively the Faradaic contribution to the current response. At a fixed potential, the current response can be separated two components:

$$i(v) = k_1 v + k_2 v^{1/2}, \quad (4)$$

For analytical purposes, combining with the differential capacitance $c = dQ/dV = i/v$, we rearrange equation (4) to equation (5):

$$c = k_1 + k_2 v^{-1/2}, \quad (5)$$

where k_1 part ($b = 1$) would indicates that the current is controlled by the surface capacitive effects and k_2 part ($b = 0.5$) indicates that the current is the redox reaction controlled process. Thus, by determining k_1 and k_2, we are able to quantify the fraction of the capacitance due to each of these contributions (see Fig. 6(b and c)). This Faradaic capacitance component, k_2, clearly dominates in CoS-9h hierarchical porous nanospheres, exceeding 780 F/g. By comparing with the total stored charge, the Faradaic capacitance effects contributed 59.3% of the total capacitances ($k_1 + k_2$), 1305 F/g, which is consistent with the data presented above. Furthermore, the surface capacitance component, k_1, of CoS-9h is 525 F/g, a little more than that of 515 F/g for CoS-12h and 500 F/g for CoS-7h. The result is consistent with the trend of specific surface area: 145 m^2/g for CoS-9h, 140 m^2/g for CoS-12h, 132 m^2/g for CoS-7h, shown in Fig. 6(d). The total stored charge in our samples can be separated into three components: 1) double layer charging of nanoparticle surfaces, 2) the faradic contribution from the charge-transfer process with surface atoms, 3) the faradic contribution from the OH^- insertion process. Here, the surface capacitance component includes double layer and surface OH^- reaction while the faradaic contribution derived from surface OH^- reaction and OH^- insertion. In view of the timeline of sulphidation, the surface capacitances derived from electric double layer effect have linear relation with surface area since 7 h of sulphidation time. The CoS nanostructures with higher specific surface area offer higher double layer capacitance.

4. Conclusion

The pseudocapacitive properties of CoS-9h-HPNs are superior to that of many cobalt sulfides based electrode materials for supercapacitors (see Table S2, [3,10–30]) and particularly the SSA of CoS-9h-HPNs is the highest among them all. The largely improved electrochemical performance might be mainly attributed to the unique CoS-9h-HPNs architecture. On one hand, the outer CoS-9h shell composed of tiny and low-crystallinity nanocrystals possesses high specific surface area and the ions in electrolyte could get through the shell efficiently for redox reaction during charge and discharge process. On the other hand, this amorphous construction may facilitate ions to transport between particles which induce very low charge transfer resistances. Lastly, the distinctive hierarchical porous structure could considerably expand the active surface area and enhance the integrity of nanospheres. As a result, the specific capacitance, rate capability, and cycling stability are significantly improved.

In conclusion, the formation mechanism of the cobalt sulfide hierarchical porous structure could be explained with proposed Brownian snowball mechanism and the CoS shell outward growth regularity may be attributed to the difference in diffusion rates of Co^{2+} and S^{2-} ions which is confirmed by the first-principles calculations. The cobalt sulfide hierarchical porous nanospheres with a specific surface area of approximately 140 m^2/g demonstrate a specific capacitance of 932 F/g at a current density of 5 A/g. The capacitance reflect a hybrid electrical energy storage mechanism and is separated into double layer charging and the Faradaic contribution from the OH^- ions reactions with surface atoms of active materials. Further, compared with the total stored charge, the Faradaic capacitance effects contributed 58.6% of the total capacitances, 1310 F/g. This work offers a method for tractable fabrication of hierarchical porous structures of simple or complex transition metal sulfides for various applications and using first-principle calculation is very effective in explaining formation mechanism which facilitate precise control of CoS-HPNs.

Acknowledgements

The authors would like express gratitude for the grants from the National Natural Science Foundation of China (NSFC—No. 51572145). Yu Cheng Zhao acknowledges the grants from China Scholarship Council for the opportunity to continue this research at Massachusetts Institute of Technology. Zhe Shi acknowledges the Research Assistant grant at the Department of Materials Science and Engineering at MIT. The authors would also like to thank Mr. David Sheehan at AkzoNobel for providing Ketjenblack. The computing resource was allocated by the RU cluster at MIT. Ju Li, Zhe Shi and Liu Min Suo acknowledge support by NSF ECCS-1610806.

Appendix A. Supplementary data

Supplementary data to this article can be found online at https://doi.org/10.1016/j.jpowsour.2018.11.055.

References

[1] T.A. Pecoraro, R.R. Chinanelli, Hydrodesulfurization catalysis by transition metal sulfides, J. Catal. 67 (1981) 430–445.
[2] H.K. Mulmudi, S.K. Batabyal, et al., Solution processed transition metal sulfides: application as counter electrodes in dye sensitized solar cells (DSCs), Phys. Chem. Chem. Phys. 13 (2011) 19307–19309.
[3] S.J. Bao, C.M. Li, C.X. Guo, Y. Qiao, Biomolecule-assisted synthesis of cobalt sulfide nanowires for application in supercapacitors, J. Power Sources 180 (2008) 676–681.
[4] P. Simon, Y. Gogotsi, Materials for electrochemical capacitors, Nat. Mater. 7 (2008) 845–854.
[5] M.H. Oh, et al., Galvanic replacement reactions in metal oxide nanocrystals, Science 340 (2013) 964–968.
[6] B.E. Conway, Electrochemical Supercapacitors: Scientific Fundamentals and Technological Applications, Kluwer, 1999.
[7] R.F. Service, New 'supercapacitor' promises to pack more electrical punch, Science 313 (2006) 902–905.
[8] M. Armand, J.M. Tarascon, Building better batteries, Nature 451 (2008) 652–657.
[9] J.R. Miller, P. Simon, Electrochemical capacitors for energy management, Science 321 (2008) 651–652.
[10] Q.H. Wang, et al., Co_3S_4 hollow nanospheres grown on graphene as advanced electrode materials for supercapacitors, J. Mater. Chem. 22 (2012) 21387–21391.
[11] X.Q. Meng, et al., Cobalt sulfide/graphene composite hydrogel as electrode for high-performance pseudocapacitors, Sci. Rep. 6 (2016) 21717.
[12] H.Z. Wan, et al., Cobalt sulfide nanotube arrays grown on FTO and graphene membranes for high-performance supercapacitor application, Appl. Surf. Sci. 311 (2014) 793–798.
[13] H. Hu, Y. Guan, X.W. Lou, Construction of complex cobalt sulfide hollow structures with enhanced electrochemical properties for hybrid supercapacitors, Inside Chem. 1 (2016) 102–113.
[14] D.P. Dubal, G.S. Gund, C.D. Lokhande, R. Holze, Controlled growth of CoS_x nanostrip arrays (CoS_x -NSA) on nickel foam for asymmetric supercapacitors, Energy Technol. 2 (2014) 401–408.
[15] P. Justin, G.R. Rao, Cobalt sulfide spheres for high-rate electrochemical capacitive energy storage application, Int. J. Hydrogen Energy 35 (2010) 9709–9715.
[16] M. Jin, et al., Different distribution of in-situ thin carbon layer in hollow cobalt sulfide nanocages and their application for supercapacitors, J. Power Sources 341 (2017) 294–301.
[17] F. Tao, Y.Q. Zhao, G.Q. Zhang, H.L. Li, Electrochemical characterization on cobalt sulfide for electrochemical supercapacitors, Electrochem. Commun. 9 (2007) 1282–1287.
[18] R.S. Ray, B. Sarma, A.L. Jurovitzki, M. Misra, Fabrication and characterization of titania nanotube/cobalt sulfide supercapacitor electrode in various electrolytes, Chem. Eng. J. 260 (2015) 671–683.
[19] Q.H. Wang, et al., Facile synthesis and superior supercapacitor performances of three-dimensional cobalt sulfide hierarchitectures, CrystEngComm 13 (2011) 6960-6093.
[20] C.Z. Yuan, L.F. Shen, F. Zhang, X.J. Lu, D.K. Li, X.G. Zhang, J. Colloid Interface Sci. 349 (2010) 181–185.
[21] S.G. Liu, et al., Facile Synthesis of novel networked ultralong cobalt sulfide nanotubes and its application in supercapacitors, ACS Appl. Mater. Interfaces 7 (2015) 25568–25573.
[22] L.S. Fa, et al., Formation of nickel cobalt sulfide ball-in-ball hollow spheres with enhanced electrochemical pseudocapacitive properties, Nat. Commun. 6 (2015) 6694.
[23] H.Z. Wan, et al., Hydrothermal synthesis of cobalt sulfide nanotubes: the size control and its application in supercapacitors, J. Power Sources 243 (2013) 396–402.
[24] Y. Liu, J.Y. Zhou, W.B. Fu, P. Zhang, X.J. Pan, E.Q. Xie, In situ synthesis of CoS_x@carbon core-shell nanospheres decorated in carbon nanofibers for capacitor electrodes with superior rate and cycling performances, Carbon 114 (2017) 187–197.

[25] R. Ren, et al., Metallic CoS_2 nanowire electrodes for high cycling performance supercapacitors, Nanotechnology 26 (2015) 494001.
[26] B. You, N. Jiang, M.L. Sheng, Y.J. Sun, Microwave vs. solvothermal synthesis of hollow cobalt sulfide nanoprisms for electrocatalytic hydrogen evolution and supercapacitors, Chem. Commun. 51 (2015) 4252.
[27] S.J. Peng, et al., MS_2 (M = Co and Ni) hollow spheres with tunable interiors for high-performance supercapacitors and photovoltaics, Adv. Funct. Mater. 24 (2014) 2155–2162.
[28] F.L. Luo, J. Li, H.Y. Yuan, D. Xiao, Rapid synthesis of three-dimensional flower-like cobalt sulfide hierarchitectures by microwave assisted heating method for high-performance supercapacitors, Electrochim. Acta 123 (2014) 183–189.
[29] Z. Yang, C.Y. Chen, H.T. Chang, Supercapacitors incorporating hollow cobalt sulfide hexagonal nanosheets, J. Power Sources 196 (2011) 7874–7877.
[30] L. Zhang, H.B. Wu, X.W. Lou, Unusual CoS_2 ellipsoids with anisotropic tube-like cavities and their application in supercapacitors, Chem. Commun. 48 (2012) 6912–6914.
[31] Y.C. Zhao, C.A. Wang, Extremely facile synthesis of manganese dioxide-polyaniline nano-reticulation with enhanced electrochemical properties, J. Alloy. Comp. 677 (2016) 281–287.
[32] Y.C. Zhao, S. Li, C.A. Wang, Manganous-manganic Oxide@Carbon core-shell nanorods for supercapacitors with high cycle retention, ECS J. Solid State Sci. Technol. 5 (2016) M5–M11.
[33] Y.C. Zhao, C.A. Wang, Nano-network MnO_2/polyaniline composites with enhanced electrochemical properties for supercapacitors, Mater. Des. 97 (2016) 512–518.
[34] G. Kresse, J. Furthmüller, Efficient iterative schemes for ab initio total-energy calculations using a plan-wave basis set, Phys. Rev. B 54 (1996) 11169–11186.
[35] J.P. Perdew, K. Burke, M. Ernzerhof, Generalized gradient approximation made simple, Phys. Rev. Lett. 77 (1996) 3865–3868.
[36] P.E. Blöchl, Projector augmented-wave method, Phys. Rev. B 50 (1994) 17953–17979.
[37] H.J. Monkhorst, J.D. Pack, Special points for Brillouin-zone integrations, Phys. Rev. B 13 (1976) 5188–5192.
[38] G. Henkelman, B.P. Uberuaga, H. Jónsson, A climbing image nudged elastic band method for finding saddle points and minimum energy paths, J. Chem. Phys. 113 (2000) 9901–9904.
[39] T.C. Liu, W.G. Pell, B.E. Conway, S.L. Roberson, Behavior of molybdenum nitrides as materials for electrochemical capacitors: Comparison with ruthenium oxide, J. Electrochem. Soc. 145 (1998) 1882–1888.
[40] J. Wang, J. Polleux, J. Lim, B. Dunn, Pseudocapacitive contributions to electrochemical energy storage in TiO_2 (Anatase) nanoparticles, J. Phys. Chem. C 111 (2007) 14925–14931.
[41] K. Brezesinski, et al., Pseudocapacitive contributions to charge storage in highly ordered mesoporous group V transition metal oxides with iso-oriented layered nanocrystalline domains, J. Am. Chem. Soc. 132 (2010) 6982–6990.
[42] V. Augustyn, et al., High-rate electrochemical energy storage through Li^+ intercalation pseudocapacitance, Nat. Mater. 12 (2013) 518–522.
[43] S. Miyazaki, M. Shirai, N. Suzuki, Electronic band structure of antiferromagnetic spinel Co_3S_4, J. Magn. Magn Mater. 177 (1998) 1367–1368.

Journal of Power Sources 414 (2019) 317

Contents lists available at ScienceDirect

Journal of Power Sources

journal homepage: www.elsevier.com/locate/jpowsour

Corrigendum

Corrigendum to "Brownian-snowball-mechanism-induced hierarchical cobalt sulfide for supercapacitors" [J. Power Sources 412 (1 February 2019) 321–330]

Yucheng Zhao[a,c], Zhe Shi[c], Tianquan Lin[c,d], Liumin Suo[c], Chao Wang[c], Jing Luo[a], Zhangshun Ruan[a], Chang-An Wang[a,*], Ju Li[b,c]

[a] State Key Lab of New Ceramics and Fine Processing, School of Materials Science and Engineering, Tsinghua University, Beijing, 100084, PR China
[b] Department of Nuclear Science and Engineering, Massachusetts Institute of Technology, Cambridge, MA, 02139, USA
[c] Department of Materials Science and Engineering, Massachusetts Institute of Technology, Cambridge, MA, 02139, USA
[d] State Key Laboratory of High Performance Ceramics and Superfine Microstructure, Shanghai Institute of Ceramics, Chinese Academy of Sciences, Shanghai, 200050, PR China

The authors regret that an error occurred in the Graphical Abstract of the published article indicated above. The Sulphur in the key should be 2- rather than 2 + and should appear as shown in the corrected figure below.

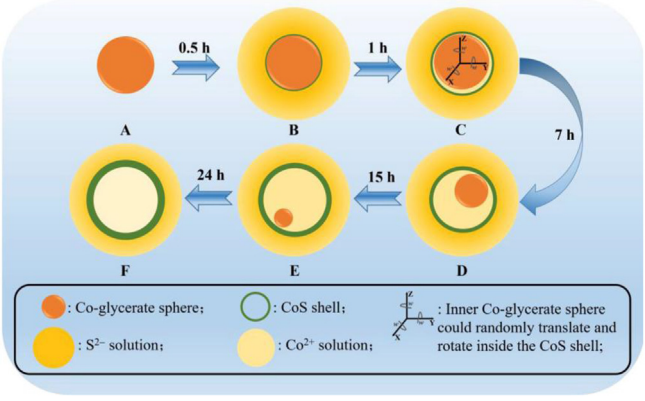

The authors would like to apologise for any inconvenience caused.

DOI of original article: https://doi.org/10.1016/j.jpowsour.2018.11.055
* Corresponding author.
E-mail address: wangca@mail.tsinghua.edu.cn (C.-A. Wang).

https://doi.org/10.1016/j.jpowsour.2019.01.023